Ultra-high contrast retinal display system for single photoreceptor psychophysics

NIKLAS DOMDEI,[1,4] LENNART DOMDEI,[1,2,4] JENNY L. REINIGER,[1] MICHAEL LINDEN,[1] FRANK G. HOLZ,[1] AUSTIN ROORDA,[3] AND WOLF M. HARMENING[1]

[1]*Department of Ophthalmology, University of Bonn, Germany*
[2]*Institute for Experimental Physics, University of Düsseldorf, Germany*
[3]*School of Optometry and Vision Science Graduate Group, University of California, Berkeley, USA*
[4]*Equal contribution first authors*
*wolf.harmening@ukbonn.de

Abstract: Due to the enormous dynamic range of human photoreceptors in response to light, studying their visual function in the intact retina challenges the stimulation hardware, specifically with regard to the displayable luminance contrast. The adaptive optics scanning laser ophthalmoscope (AOSLO) is an optical platform that focuses light to extremely small retinal extents, approaching the size of single photoreceptor cells. However, the current light modulation techniques produce spurious visible backgrounds which fundamentally limit experimental options. To remove unwanted background light and to improve contrast for high dynamic range visual stimulation in an AOSLO, we cascaded two commercial fiber-coupled acousto-optic modulators (AOMs) and measured their combined optical contrast. By compensating for zero-point differences in the individual AOMs, we demonstrate a multiplicative extinction ratio in the cascade that was in accordance with the extinction ratios of both single AOMs. When latency differences in the AOM response functions were individually corrected, single switch events as short as 50 ns with radiant power contrasts up to $1:10^{10}$ were achieved. This is the highest visual contrast reported for any display system so far. We show psychophysically that this contrast ratio is sufficient to stimulate single foveal photoreceptor cells with small and bright enough visible targets that do not contain a detectable background. Background-free stimulation will enable photoreceptor testing with custom adaptation lights. Furthermore, a larger dynamic range in displayable light levels can drive photoreceptor responses in cones as well as in rods.

References and links

1. J. Liang, D. R. Williams, and D. T. Miller, "Supernormal vision and high-resolution retinal imaging through adaptive optics," J. Opt. Soc. Am. A **14**(11), 2884–2892 (1997).
2. D. R. Williams, "Imaging single cells in the living retina," Vision Res. **51**(13), 1379–1396 (2011).
3. A. Roorda, "Adaptive optics for studying visual function: A comprehensive review," J. Vis. **11**(7), 1–21 (2011).
4. L. C. Sincich, Y. Zhang, P. Tiruveedhula, J. C. Horton, and A. Roorda, "Resolving single cone inputs to visual receptive fields," Nat. Neurosci. **12**(8), 967–969 (2009).
5. E. A. Rossi and A. Roorda, "The relationship between visual resolution and cone spacing in the human fovea," Nat. Neurosci. **13**(2), 156–157 (2010).
6. W. M. Harmening, W. S. Tuten, A. Roorda, and L. C. Sincich, "Mapping the Perceptual Grain of the Human Retina," J. Neurosci. **34**(16), 5667–5677 (2014).
7. M. A. Mainster, G. T. Timberlake, R. H. Webb, and G. W. Hughes, "Scanning laser ophthalmoscopy. Clinical applications," Ophthalmology **89**(7), 852–857 (1982).
8. D. W. Arathorn, Q. Yang, C. R. Vogel, Y. Zhang, P. Tiruveedhula, and A. Roorda, "Retinally stabilized cone-targeted stimulus delivery," Opt. Express **15**(21), 13731–13744 (2007).
9. Q. Yang, D. W. Arathorn, P. Tiruveedhula, C. R. Vogel, and A. Roorda, "Design of an integrated hardware interface for AOSLO image capture and cone-targeted stimulus delivery," Opt. Express **18**(17), 17841–17858 (2010).
10. A. Stockman and L. T. Sharpe, "Into the twilight zone: the complexities of mesopic vision and luminous efficiency," Ophthalmic Physiol. Opt. **26**(3), 225–239 (2006).

11. B. E. A. Saleh and M. C. Teich, "Acousto-optics," in *Fundamentals of Photonics* (John Wiley & Sons, Inc., 1991).
12. S. Poonja, S. Patel, L. Henry, and A. Roorda, "Dynamic visual stimulus presentation in an adaptive optics scanning laser ophthalmoscope," J. Refract. Surg. **21**(5), S575–S580 (2005).
13. K. Grieve, P. Tiruveedhula, Y. Zhang, and A. Roorda, "Multi-wavelength imaging with the adaptive optics scanning laser Ophthalmoscope," Opt. Express **14**(25), 12230–12242 (2006).
14. A. B. Watson and D. G. Pelli, "QUEST: a Bayesian adaptive psychometric method," Percept. Psychophys. **33**(2), 113–120 (1983).
15. K. S. Bruce, W. M. Harmening, B. R. Langston, W. S. Tuten, A. Roorda, and L. C. Sincich, "Normal Perceptual Sensitivity Arising From Weakly Reflective Cone Photoreceptors," Invest. Ophthalmol. Vis. Sci. **56**(8), 4431–4438 (2015).
16. R. Sabesan, B. P. Schmidt, W. S. Tuten, and A. Roorda, "The elementary representation of spatial and color vision in the human retina," Sci. Adv. **2**(9), e1600797 (2016).
17. W. S. Tuten, W. M. Harmening, R. Sabesan, A. Roorda, and L. C. Sincich, "Spatiochromatic Interactions between Individual Cone Photoreceptors in the Human Retina," J. Neurosci. **37**(39), 9498–9509 (2017).
18. E. A. Rossi, R. L. Achtman, A. Guidon, D. R. Williams, A. Roorda, D. Bavelier, and J. Carroll, "Visual function and cortical organization in carriers of blue cone monochromacy," PLoS One **8**(2), e57956 (2013).
19. N. Domdei, F. G. Holz, A. Roorda, L. C. Sincich, and W. M. Harmening, "Characterization of an adaptive optics SLO based retinal display for cellular level visual psychophysics," Perception **44**, 1–415 (2015).
20. M. Bach, T. Meigen, and H. Strasburger, "Raster-scan cathode-ray tubes for vision research--limits of resolution in space, time and intensity, and some solutions," Spat. Vis. **10**(4), 403–414 (1997).
21. M. Ghodrati, A. P. Morris, and N. S. C. Price, "The (un)suitability of modern liquid crystal displays (LCDs) for vision research," Front. Psychol. **6**, 303 (2015).
22. H. Ito, M. Ogawa, and S. Sunaga, "Evaluation of an organic light-emitting diode display for precise visual stimulation," J. Vis. **13**(7), 6–21 (2013).
23. E. Geissler, C. Nieten, G. Rudolph, and M. Pretorius, "Projektionssystem," U.S. patent EP 2294483 B1 (2009).
24. K. Petermann, "Laser diode modulation and noise," in *Advances in Optoelectronics* (Kluwer Academic Publishers, 2012), pp. 78–114.
25. A. Stockman, D. I. A. MacLeod, and N. E. Johnson, "Spectral sensitivities of the human cones," J. Opt. Soc. Am. A **10**(12), 2491–2521 (1993).
26. M. Roth, M. Tseitlin, and N. Angert, "Oxide Crystals for Electro-Optic Q -Switching of Lasers," Glass Phys. Chem. **31**(1), 86–95 (2005).
27. D. Koenig and H. Hofer, "The absolute threshold of cone vision," J. Vis. **11**(1), 21–24 (2011).
28. J. N. Tinsley, M. I. Molodtsov, R. Prevedel, D. Wartmann, J. Espigulé-Pons, M. Lauwers, and A. Vaziri, "Direct detection of a single photon by humans," Nat. Commun. **7**, 12172 (2016).
29. H. D. Crane and C. M. Steele, "Generation-V dual-Purkinje-image eyetracker," Appl. Opt. **24**(4), 527–537 (1985).
30. D. H. Brainard, D. R. Williams, and H. Hofer, "Trichromatic reconstruction from the interleaved cone mosaic: Bayesian model and the color appearance of small spots," J. Vis. **8**, 15–23 (2008).
31. Q. Wang, W. S. Tuten, B. J. Lujan, J. Holland, P. S. Bernstein, S. D. Schwartz, J. L. Duncan, and A. Roorda, "Adaptive optics microperimetry and OCT images show preserved function and recovery of cone visibility in macular telangiectasia type 2 retinal lesions," Invest. Ophthalmol. Vis. Sci. **56**(2), 778–786 (2015).
32. W. S. Tuten, P. Tiruveedhula, and A. Roorda, "Adaptive optics scanning laser ophthalmoscope-based microperimetry," Optom. Vis. Sci. **89**(5), 563–574 (2012).
33. R. W. Massof and D. Finkelstein, "Rod sensitivity relative to cone sensitivity in retinitis pigmentosa," Invest. Ophthalmol. Vis. Sci. **18**(3), 263–272 (1979).
34. R. G. Fraser, R. Tan, L. N. Ayton, E. Caruso, R. H. Guymer, and C. D. Luu, "Assessment of retinotopic rod photoreceptor function using a dark-adapted chromatic perimeter in intermediate age-related macular degeneration," Invest. Ophthalmol. Vis. Sci. **57**(13), 5436–5442 (2016).
35. R. W. Nygaard and R. A. Schuchard, "SLO radiant power and brightness," J. Rehabil. Res. Dev. **38**(1), 123–128 (2001).
36. A. Stockman and L. T. Sharpe, "The spectral sensitivities of the middle- and long-wavelength-sensitive cones derived from measurements in observers of known genotype," Vision Res. **40**(13), 1711–1737 (2000).

1. Introduction

Human vision starts in the mosaic of retinal photoreceptors, cones and rods, where the stream of incident photons is captured and converted into neurochemical signals which form the basis of visual perception. With recent advances in high-resolution ophthalmoscopy, the retinal photoreceptor mosaic can be resolved and imaged in the living subject, opening the door to assess the retina's structural as well as its functional architecture *in vivo* [1–3]. In particular, the adaptive optics scanning laser ophthalmoscope (AOSLO) is an optical platform that can deliver light to targeted retinal areas with microscopic precision, enabling physiological and psychophysical visual function testing on a cellular scale [4–6].

In a scanning system such as the AOSLO, spatially resolved visual stimuli are generated by temporal modulation of a visible laser beam swept across the retina of an observer, reminiscent of the temporal modulation of an electron beam in a cathode ray tube to create a visual display [7]. For instance, a square stimulus with maximum visual contrast is rendered by turning on the stimulation light for the time the scanning beam needs to sweep across a retinal area that corresponds to the stimulus' visual features, and turning it off for the remaining time (Fig. 1(A)). In such a display, visual contrast is governed by the temporal modulation characteristics of the light switch. Because AOSLO systems operate with scanning line rates in the Kilohertz range, light switching needs to be fast if stimuli of high spatial resolution (with their size usually being just a fraction of a complete line scan) are desired [8,9]. Acousto-optic modulators (AOMs) provide the necessary bandwidth (typically above 100 Megahertz) to achieve nanosecond-scale switching events independent of wavelength, and are therefore the method of choice for today's AOSLO imaging and stimulation devices.
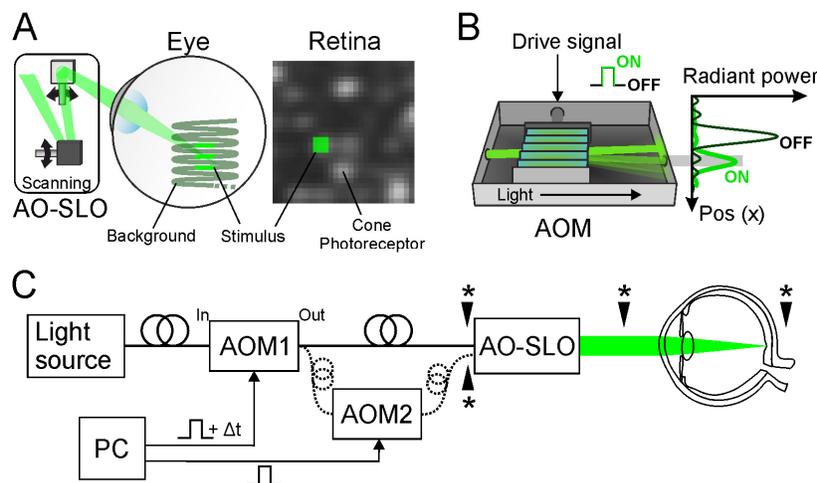

Fig. 1. High-contrast *in vivo* micro-stimulation for visual psychophysics. A: With AOSLO, single photoreceptors can be imaged and targeted for small spot stimulation. During scanning (horizontal and vertical arrows), incomplete extinction of stimulus light modulation will produce stimuli on the subject's retina that contain a visible background, limiting experimental options. B: Acousto-optic modulation exhibits finite extinction, i.e. the ratio of light transmitted during full ON and OFF is limited by light leak caused by incomplete optical isolation between the undiffracted (black) and the modulated diffracted beam (green, gray area in power plot, not to scale). C: AOM cascading schematic. Intensity of a visible stimulation light is controlled by fiber-coupled acousto-optic modulation (AOM) in single (solid) or cascaded (dashed) configuration to produce diffraction limited spatially resolved stimuli on the retina of a human observer. Temporal alignment is realized by delaying drive signals (Δt) for AOM1. We analyzed visual contrast of the stimulus light either radiometrically or psychophysically at the locations marked with an asterisk. Cascading increased contrast multiplicatively and removed unwanted backgrounds.

Acousto-optic light modulation, however, comes at the cost of incomplete extinction: Even when an AOM is off, some amount of light "leaks" through its output due to imperfect optical isolation of the modulated diffraction pattern (Fig. 1(B)). Commercially available AOMs are specified with maximum extinction ratios of around 40 dB, i.e. the radiant power ratio at their modulated output between OFF and ON, or simply their optical contrast, covering an illumination range of around 11 log units for cones and rods combined [10], the contrast of today's AOMs set a fundamental limit to stimulation capabilities. AOM leakage creates a constant background illumination, with an extent coinciding with the SLO scanning field. In consequence, measures of visual sensitivity, for instance, can only be performed as

light increments against a visible background, with the stimulus and background being comprised of the same wavelength (Fig. 1). If small visual stimuli are desired (e.g. when single cones are tested), stimulus light levels need to be high, and in turn, background levels will be high as well. At higher eccentricities, on the other hand, visual stimuli are not bright enough to trigger perception. Moreover, high background light intensities will saturate rods, making it impossible to assess them psychophysically [6].

We describe a simple solution how to achieve background light elimination and greater dynamic range for the stimulus light for SLO-based psychophysics (Fig. 1(C)). By cascading and temporally aligning two fiber-coupled AOMs, we demonstrate radiometrically and psychophysically that this approach extends current AOSLO testing regimes into the mesopic and full scotopic range. In general, AOM cascading may be useful in all fields requiring light modulation with extremely high visual contrast ratios.

2. Materials and methods

To determine the limits of optical contrast produced with an acousto-optic switched retinal display, we first characterized the contrast of single and cascaded fiber-coupled AOMs by measuring their radiometric power outputs as a function of drive voltages. After identifying zero-point location and latency for each AOM individually, temporal alignment (i.e. concurrent switching times), was verified in an AOSLO system. For functional testing of single photoreceptors, we fitted a multi-wavelength AOSLO setup with a temporally aligned AOM cascade to produce small visual targets for psychophysical testing and measured background light visibility and small spot thresholds in two human observers.

Acousto-optic light modulation and radiometry

In AOMs, contrast limits arise due to their mode of operation. Briefly, light intensity modulation is achieved through light diffraction in an oscillating crystal. Piezo elements attached to one side of a photonic crystal (in our case: Tellurium dioxide) induce travelling ultrasonic waves within the crystal. The oscillating crystal forms a spatially resolved pattern of local density changes that acts as an optical lattice by which an incident optical beam is diffracted. While most light propagates through the lattice undiffracted, some light will be diffracted under a flat angle (the Bragg-angle), and can be collected at the AOM's output. In theory, the amplitude of that modulated portion and hence the radiant power output, P, of an AOM depends on the piezo drive voltage, U, following a $\sin^2$ - function [11]:

$$P(U) = P_{max} \cdot \sin\left(\frac{U - U_{min}}{U_{max} - U_{min}} \cdot \frac{\pi}{2}\right)^2 + P_{min} \tag{1}$$

U_{max} is the drive voltage to generate the maximum output power P_{max}. Increasing drive voltage and thus increasing ultrasonic wave amplitude will cause higher efficiency of the optical lattice, which in turn leads to more power at the AOM output. P_{min} describes the minimum output power at U_{min}, which is non-zero and defines the amount of light leaked at this driving voltage. P_{min} being non-zero is due to the fact that light inevitably falls into the output path of the AOM. This occurs because of light scattering within the crystal and optical components. Moreover, because the Bragg angle is relatively flat, the first order maximum of the deflected light path and the Airy disc of the undiffracted light path overlap (Fig. 1(B)). Since P_{max}, U_{max}, P_{min} and U_{min} are values inherent to the exact optomechanical setup, crystal medium and wavelength tuning of the AOM, they have to be determined empirically by direct measurement of radiant power at its output.

In our experiments we used two commercially available fiber-coupled AOMs with 250 MHz bandwidth, with highest efficiency at a wavelength of 545 nm (Model TEM-250-50-10-2FP *with* high extinction option, Brimrose, Maryland, USA). Since each AOM device and driver unit are tuned individually by the manufacturer to achieve maximal extinction ratios,

their modulation characteristics will be different and have to be measured individually. To that end, we first recorded each AOM's radiant output power at steady state drive voltages separately and combined (by cascading them). The cascade is setup by feeding the modulated output of one AOM into the input of a second AOM. The resulting radiant power was measured at the second AOM's fiber output with a silicon photodiode attached to a benchtop power meter (Standard probe: S121C, high sensitive probe: S130C, Power meter: PM320E, Thorlabs, Inc., Newton, New Jersey, USA). Steady-state drive voltages between 0 and 1000 mV with 25 mV steps were produced with a digital signal generator (Model 33500B, Keysight Technologies, Inc., Santa Rosa, California, USA). The results of each AOM were used to calculate a look-up-table (LUT) to linearize AOM output individually for further testing in our AOSLO setup. Mapping of AOM drive signals to the voltage needed to achieve a constant output power was expressed in arbitrary units. A drive signal of 1.0 produced maximum power at the AOM's output, a value of 0.0 produced minimum power. A drive signal of 0.5, for instance, produced half of the maximum output power. Light source for all experiments was a supercontinuum laser (SuperK Extreme EXR-15, NKT Photonics, Birkerød, Denmark), spectrally filtered to output light in two distinct fiber-coupled channels with center wavelengths of 543 nm ($\pm$ 12 nm) for stimulus presentation and 840 nm ($\pm$ 25 nm) for retinal imaging.

Temporal alignment and AOSLO micro stimulation

The AOSLO is an optical instrument that can resolve and target individual photoreceptor cells of the living retina for functional testing. The details of AOSLO stimulation procedures have been described elsewhere [6,8,12,13]. Briefly, a focused beam scans across the retina creating a square field in which visible stimuli can be created (retinal display). Stimuli are rendered directly on the retina by temporal modulation of the beam's intensity. This is achieved either by reducing the intensity of the imaging wavelength to form spatially resolved stimuli with negative contrast polarity ('black' against a visible imaging field), or by modulation increments of a dedicated stimulation wavelength for positive contrast polarity stimuli (colored on same color background), or a combination thereof (Fig. 1(C)).

In order to successfully cascade two AOMs for our experiments, each AOM had to be controlled via individual drive signals. This is due to differences in zero-point location (U_{min} of Eq. (1)) and signal latency, which are idiosyncratic to the AOM. Thus, both units had to be measured separately before they were integrated into the AOSLO system. Zero-point location was determined by adjusting the voltage of each AOM's drive input in 1 mV steps until the radiant power reached a minimum. AOM latency was measured as the elapsed time between the onset of a bar stimulus producing drive signal (comparable to a 5 MHz square-wave drive signal with 10 ns slopes formed by a digital signal generator) and the onset of a voltage change of a high-speed photodetector (Model FPD510-FV, Menlo Systems GmbH, Martinsried, Germany) placed at the AOM fiber output. Latency signals were recorded with a digital oscilloscope (Model MSO-X 3054A, Agilent Technologies, Inc., Santa Clara, California, USA) and analyzed with Matlab (R2014a, The Mathworks, Inc., Natick, MA, USA). Latency measurements are given as the mean of 7 repeated onset events.

After determining zero-point location and latency for each AOM individually, temporal alignment (i.e. concurrent switching times) was verified in the AOSLO system. Therefore, AOM drive signals were produced by a field programmable gate array (FPGA) board (Model ML-506, Xilinx, San Jose, USA) that ran in synchrony with the AOSLO's scanning mirrors [9]. This added spatial control to the stimulus geometry, enabling stimulus presentation by definition of pixel coordinates in reference to collected AOSLO images. Because the resonant scanner of the AOSLO operates at 16 kHz, one line of our imaging and stimulation system (512x512 pixels) was generated in 25 µs. Scan reversals were omitted, resulting in a 40% duty cycle of the AOM driver signal. Due to the sinusoidal velocity profile of the resonant scanner during a cycle, laser sweep time across a retinal area corresponding to one image

pixel was not constant. Close to the reversal points of the scan line, the area corresponding to one image pixel was traversed in about 160 ns, whereas in the center of the field travel time was considerably shorter (40 ns per pixel). Because the pixel clock of the employed signal generator for the AOSLO system (FPGA board) ran at 20 MHz, the resulting computational step size was 50 ns, limiting tests to larger (i.e. longer) stimuli: 2, 3 and 5 pixel squares were chosen.

AOM latency correction was verified in our AOSLO system by recording images of the square stimuli with a CCD camera (Model GS3-U3-15S5M-C, FLIR Integrated Imaging Solutions, Inc., Richmond, British Columbia, Canada), positioned in a retinal plane of the system's beam path. The camera's digital shutter was adjusted to capture a single AOSLO frame (~33 msec). For later analysis, 90 frames were captured and an averaged image was computed. We compared stimulus intensities in the average frame by calculating the sum of all pixel values within a cropped area of the whole frame around the stimulus location (Fig. 3(C)).

Human psychophysics

We conducted psychophysical experiments in two volunteer subjects (1 female, 1 male) with no known vision abnormalities. For scotopic viewing conditions, subjects were dark adapted for at least 40 minutes. Mydriasis and cycloplegia were induced by instilling one drop of 1% Tropicamide before dark adaptation started. Written informed consent was obtained from each subject and all experimental procedures adhered to the tenets of the Declaration of Helsinki and were in accordance with the guidelines of the independent ethics committee of the medical faculty at the Rheinische Friedrich-Wilhelms-Universität of Bonn.

Three psychophysical experiments were carried out with each subject. First, a foveal and peripheral detection threshold of the 543 nm background light was determined. The AOSLO scan field was set to comprise 600 pixels per degree of visual angle, resulting in a field size of 0.85 degree of visual angle, or ~247 μm edge length on the retina (assuming an average retinal magnification of 290 μm per degree of visual angle). The light source output power and hence AOM input intensity was held constant. Measured at the plane of the cornea, maximum incident power (AOM drive signal at 1.0 a.u.) was 30 μW for single AOM and 3 μW for cascaded AOMs. Drive voltages were then set to yield minimum output power (about 10^4 and 10^{10} attenuation for single and cascaded AOMs, respectively) to produce the residual background light, calculated to carry $5.7 \cdot 10^{-10}$ W for single, and $2.5 \cdot 10^{-16}$ W of 543 nm light for cascaded AOMs. Neutral density filters were introduced into the AOSLO beam path until the scanning field became invisible during foveal and peripheral (10° nasally) inspection.

Second, having the individual attenuation for complete background elimination at the given retinal location in place, we tested small spot stimulus visibility under dark-adapted conditions. Square stimuli with edge lengths of 64, 32, 10, 5, 3 and 2 pixels were used. Stimuli were flashed at 3 Hz to minimize adaptation effects. Stimulus intensity was carefully adjusted by the operator by controlling FPGA drive signals to yield the minimum intensity detectable for each stimulus size. To avoid additional light from the 840 nm imaging and wavefront sensing channel during these two experiments, the best wavefront correction was measured before an experimental session and the deformable mirror was locked with a fixed correction until the end of the experiment. The 840 nm light was then turned off during detection experiments. Sufficient wavefront correction throughout a session was confirmed by inspecting the quality of the IR retinal image after completion of a session.

In a third experiment, we compared detection thresholds of single and cascaded AOM stimulation during typical micro-stimulation conditions. Infrared light (840 nm) was employed for imaging and closed-loop AOSLO operation, and it produced a visible background of around 3.14 cd/m^2 (~100 μW of 840 nm light at the pupil plane). Light levels for single and cascaded AOM switching in the stimulus channel (543 nm) was set to produce similar maximum power as measured at the subject's pupil plane (~1-15 nW full field, 100%

duty cycle). Despite the different contrast ratios for single and cascaded AOM switching, the 543 nm background was not visible to the subjects in both operating modes due to the brighter 840 nm imaging field. Stimulus presentation duration was set to a single frame of AOSLO image acquisition, habitual fixational eye movements were tolerated. The tested stimulus sizes were 3-by-3 pixel (stimulus duration: 62.6 µsec, stimulus size on retina: 1.21 µm or 0.25 arcmin) and 10-by-10 pixel (562.9 µsec, 4.35 µm or 0.9 arcmin). Detection thresholds were estimated using an adaptive Bayesian staircase method (QUEST Matlab toolbox from [14]), with 20 trials per run. Subjects completed 4 to 7 repeat runs per retinal location (foveal center and 10° eccentricity). Threshold estimates were expressed in arbitrary units (a.u.). For example, a threshold of 0.5 a.u. corresponds to 50% of maximum light intensity. To minimize variability in the light source output power, experiments commenced 20 minutes after the laser was turned on. To compensate for residual drift, we measured the AOM output power at maximum level at the beginning and after completion of all runs per test condition. We converted threshold estimates from arbitrary units into absolute stimulus power under the assumption of a linear power drift of the source during a single session using the exact time stamps for each test run. Linear power drift behavior of the light source was confirmed in previous measurements. Because temporal alignment of both AOMs was not perfect in our case (see results: Switching latency and temporal alignment, Fig. 3(B)), a 3x3 pixel stimulus created in the cascade carried only 90% of the total power of the same stimulus created with a single AOM at the same drive signal. For the 10x10 pixel stimulus, this value was 97%. Threshold estimates for AOM cascading relative to single AOM switching were corrected for this difference.

Statistical threshold comparison was performed with Student's t-test for paired data after confirming normal distribution (Shapiro-Wilk test) and homoscedasticity (Levene test).

3. Results

Light modulation characteristics

To characterize the contrast of single and cascaded fiber-coupled AOMs, we first measured their individual radiometric power outputs as a function of drive voltages. For that purpose, a constant input light source with 55 mW at 543 nm center wavelength was used. Generally, both AOMs showed sine-power function characteristics, but with differing exponents (Fig. 2(A)). The fit functions minimizing the sum of the residual errors were:

$$P_{AOM1}(U) = 5.50 \cdot \sin\left(\frac{U + 4.2}{1100 + 4.2} \cdot \frac{\pi}{2}\right)^2 + 1.0 \cdot 10^{-4} \tag{2}$$

$$P_{AOM2}(U) = 2.74 \cdot \sin\left(\frac{U - 38}{1050 - 38} \cdot \frac{\pi}{2}\right)^4 + 1.2 \cdot 10^{-5} \tag{3}$$

Insertion loss due to finite diffraction efficiency in each AOM was about 90%. Zero point location (i.e. the drive voltage at which the radiant power output had its minimum) differed for each AOM. AOM1 had its minimum at –4.2 mV and AOM2 at 38.0 mV. These idiosyncratic differences are to be considered, as they would lead to a non-monotonic characteristic in the cascade if left unaccounted for. Minimum output power was $1.04 \cdot 10^{-4}$ mW and $1.20 \cdot 10^{-5}$ mW for AOM1 and AOM2, respectively.
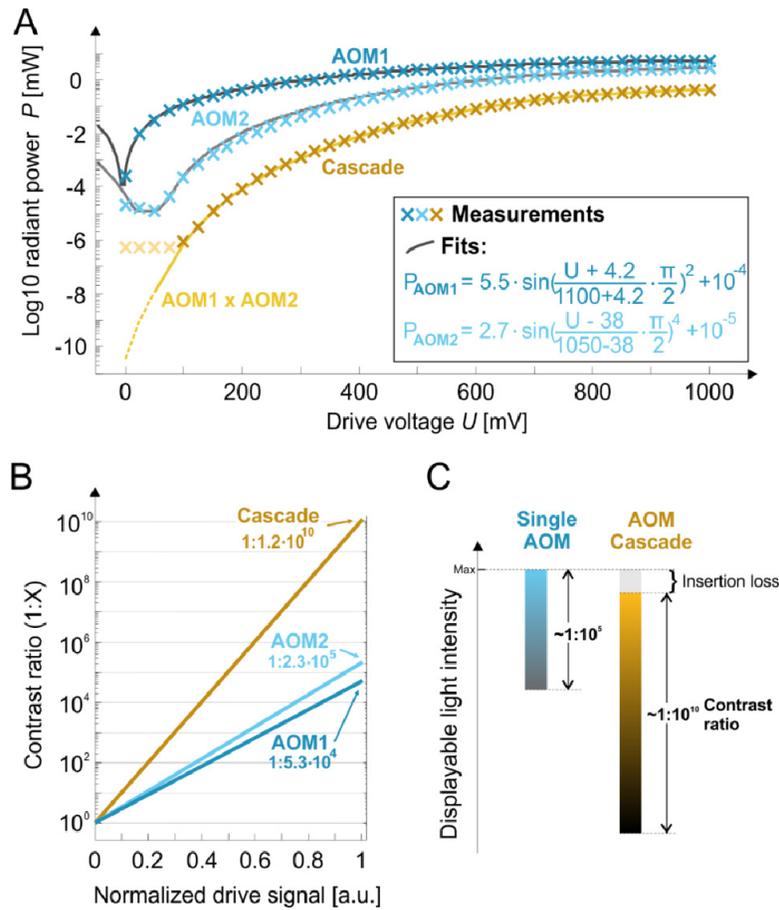
Fig. 2. Single and cascaded AOM optical contrast. A: Radiant output power as a function of drive voltage measured with individual AOMs (blue markers) were best fitted by a $\sin^2$ or $\sin^4$ function (grey lines, fit parameters given), respectively. Minimal power was found at non-zero drive signals. In the cascade, maximum absolute output power is lower (amber markers), and the characteristic closely follows multiplication of the single AOM measurement points (amber line). Our setup did not allow power measurements below 10^{-6} mW, resulting in a plateau at low drive voltages (lightly colored +'s). B: AOM contrast ratios yielded by normalization and zero-point correction of data from A after drive signal linearization. A drive signal of 1.0 a.u. produces maximum output power for each AOM, a signal of 0 the minimum. The y-axis shows the contrast ratio relative to minimum output. C: Cascading two AOMs results in a superior contrast ratio relative to single AOMs. Due to about 90% insertion loss of absolute output power in the cascade, the range of displayable light levels is shifted towards lower intensities. The effective contrast ratio of the AOM cascade was about $1:10^{10}$.

In the cascade, feeding the modulated output of AOM1 into AOM2, the measured characteristic followed the multiplied single AOM measurements with a correlation of 99.99% ($p = 4 \cdot 10^{-66}$, Pearson correlation) as expected (Fig. 2(A)). Range limits of the used photodiode demanded cascade drive signals above 100 mV. Effectively, readings levelled off at around $5 \cdot 10^{-7}$ mW. The overall light loss due to AOM cascading (irrespective of AOM order) was about 90% compared to single AOM operation.

In terms of light modulation contrast, the ratio of radiant output power between U_{min} and U_{max} is of interest. Single AOM characteristics were normalized to their maximum output power and corrected for zero point location by creating a look-up-table based on the measurements from Fig. 2(A). Individual and cascaded modulation contrast resulted in

measurements shown in Fig. 2(B). Individual AOMs achieved maximum contrast ratios of $1:5.3\cdot10^4$ (AOM1) and $1:2.3\cdot10^5$ (AOM2). The overall cascaded AOM contrast ratio was calculated to be $1:1.2\cdot10^{10}$. Ultimately, cascading two AOMs increased the displayable contrast by a factor between 10^5 and 10^6 compared to single AOM switching.
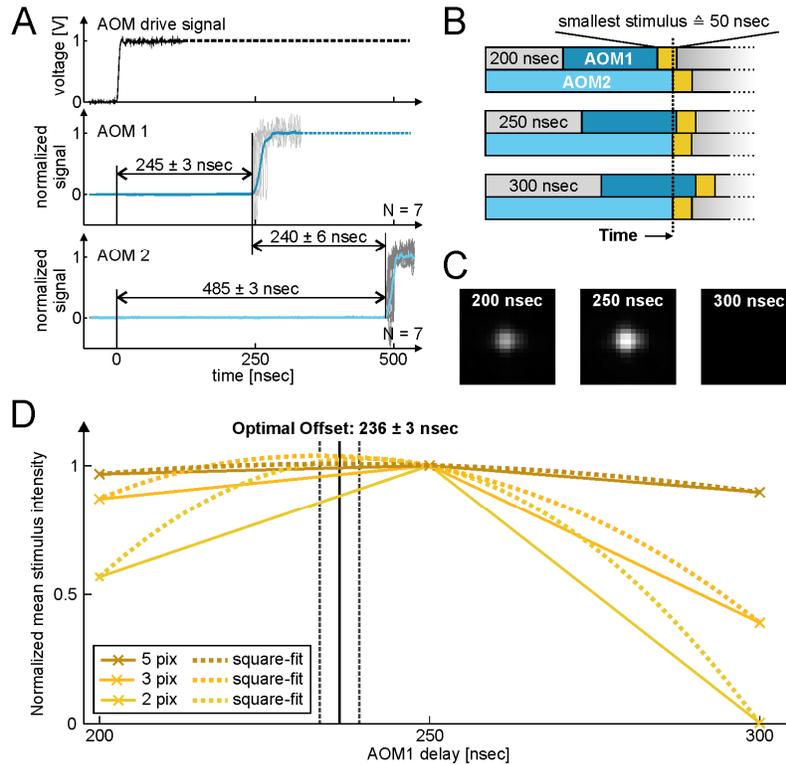

Fig. 3. AOM latency and temporal alignment. A: Single AOM response functions (middle and lower row, grey: single measurement, blue: average) measured after repeated (n = 7) square wave drive signal onsets (upper row). Mean latency (± STD) values are shown in the plot, latency difference between the two AOMs was 240 ± 6 ns. B: To temporally align AOM switching events for small visual stimuli, drive signals for AOM1 were delayed in 50 ns increments, to a close-to-optimal delay at around 250 ns. C: Average of 90 frames captured with a CCD-camera at a retinal plane of the AOSLO with varying AOM delays for a 50 ns stimulus (2x2 pixel). D: Optimal delay analysis with different stimulus sizes based on image intensity as in C. Cross markers are data points (connecting solid lines added for visibility), exponential fit functions (power of two, dotted lines) locate the optimal offset to be 236 ± 3 ns, in agreement with the measured delay from A.

Switching latency and temporal alignment

In SLO-based applications where spatially resolved visual stimuli are rendered by temporal modulation of a scanning beam (see Methods), light switching timing is essential. If two AOMs are cascaded, both need to respond synchronously, especially if small stimuli are desired. Otherwise, uncontrolled size and intensity losses will occur. We measured single AOM latencies by detecting their optical output with a high-speed photodetector in response to repeated square-wave drive signals.

We found the latencies of our AOMs to be 245 ± 3 ns for AOM1 and 485 ± 3 ns for AOM2, resulting in an offset of 240 ± 6 ns between them (Fig. 3(A)). This temporal offset needs to be taken into account for cascaded stimulation by adding a corresponding delay for the faster AOM (AOM1). We tested how far temporal delays of 200, 250 and 300 ns would

impact stimulus geometry and intensity (Fig. 3(B)), while using small squares with edge lengths of 2, 3 and 5 pixels as stimuli. We recorded images of these stimuli with a CCD-Camera placed in a retinal plane of the AOSLO. A qualitative analysis yielded the optimal offset to be 250 ns (Fig. 3(C)). Non-overlapping drive signals (300 ns delay) resulted in extremely low stimulus intensities. When drive signals overlapped, the stimulus spot was visible with increasing size and intensity closer to the optimal 240 ns delay. For a quantitative assessment of the optimal offset, we computed the mean stimulus intensity of the three different sized stimuli while varying the offset for AOM1 (Fig. 3(D)). Again, an offset of 250 ns showed the best results, determined by the highest stimulus intensity. An x^2-fit to the three data points revealed an optimal offset of 236 ± 3 ns, which is in good accordance with the initially measured offset of 240 ± 6 ns.

Psychophysics: background extinction and small spot sensitivity

To demonstrate that the increased optical contrast in the AOM cascade has measurable consequences for visual perception, we conducted three psychophysical experiments with two human subjects. In the first experiment, subjects determined the level of light attenuation (by adding ND filters into the beam path) necessary for complete AOM leak background elimination in the AOSLO retinal display after dark adaptation. With a single AOM, S1 required attenuation of $10^{5.5}$ at the fovea and an attenuation of 10^7 at 10° eccentricity (S2: $10^{4.5}$ and $10^{6.6}$, respectively) (Fig. 4(A)). With cascaded AOMs, combining high extinction and an additional insertion loss of one log unit, both subjects were not able to perceive a background at the fovea, and an ND of $10^{0.6}$ (factor ~4) was sufficient to remove the background at eccentric fixation for both subjects. Defining the minimal attenuation needed to remove the background as detection threshold, single AOM radiant powers incident at threshold were $1.8 \cdot 10^{-15}$ W (S1) and $1.8 \cdot 10^{-14}$ W (S2) at foveal inspection, and $5.7 \cdot 10^{-17}$ W (S1) and $1.4 \cdot 10^{-16}$ W (S2) at eccentric fixation. For cascaded AOMs, a foveal threshold remains undefined because the background was never visible. At eccentric fixation, thresholds were $6.3 \cdot 10^{-17}$ W for both subjects. Converting the radiometric measurements to an equivalent photometric unit of luminous intensity (brightness) of the scan field (for a detailed calculation see Appendix), the resulting average background luminance threshold across subjects and condition was $1.19 \cdot 10^{-3}$ cd/m² for foveal and $3.90 \cdot 10^{-6}$ cd/m² for eccentric fixation.

We tested visibility of various sized stimuli in a second experiment, under conditions where the background was fully eliminated. With a single AOM, the smallest stimuli (2, 3 and 5 pixels) were either never visible or barely visible at maximum light modulation (Fig. 4(B)). With cascaded AOMs, stimuli were visible at all sizes. Visibility was even preserved at low modulation levels (inter subject average detection threshold for the 2-by-2 pixel square: 0.21 a.u. at fovea, 0.09 a.u. at 10° eccentricity), leaving a large dynamic range for visual stimulation and threshold experiments. This was the case for both foveal and eccentric fixation (Fig. 4(B)).
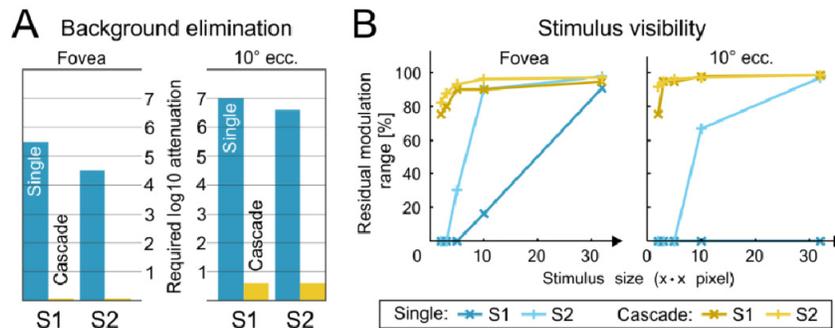
Fig. 4. Background elimination and stimulus visibility in AOSLO micro-stimulation. A: Light attenuation necessary to eliminate the AOM background leak for two dark adapted subjects (S1, S2), inspected foveally and at 10° nasal eccentricity. With single AOM modulation (blue bars), light leak was removed with an attenuation of 4.5-5.5 log units at the fovea. The background was never visible with cascaded modulation. With eccentric fixation, attenuation of 6.6-7 log units was required to remove the background for single AOM, and 0.6 log units for cascaded AOM light modulation (amber bar). B: Residual modulation range for small visible stimuli with eliminated background (i.e. viewing conditions found in A). Different sized stimuli were flashed at 3 Hz, subjects reported detection under foveal or eccentric fixation. With single AOM switching, stimuli had to be large to be visible, at both foveal and eccentric fixation (blue markers and lines). The smallest stimuli were not visible or required maximal modulation to be seen. With AOM cascading, even the smallest stimuli were easily seen, leaving a much greater dynamic range of stimulus modulation for psychophysical testing (amber markers and lines).

Finally, we tested if cascaded AOM switching can produce small spot visual stimuli with light levels that can be directly compared to prior studies that used single AOM switching [6,15–17]. We recorded sensitivity thresholds for 3 and 10 pixel square stimuli (1.21 μm and 4.35 μm on the retina, respectively) against a visible 840 nm imaging raster, which effectively masked the 543 nm background. While the stimulus appeared at a fixed position relative to the imaging raster, natural fixational eye movements were allowed to occur (see example in Fig. 5(A)). Averaged across both subjects, more than 50% of all stimuli presentations fell into a (roughly) circular area with a diameter of 5.58 arcmin, or 26.98 μm on the retina (S1: 5.66/4.92 arcmin; S2: 5.75/6.00 arcmin; single/cascaded AOMs, respectively). Thresholds were determined using an adaptive Bayesian staircase method, and threshold progression was very similar for both single and cascaded AOM stimulus presentation (see example in Fig. 5(B)). For threshold comparison between single and cascaded AOM switching, threshold estimates given in arbitrary units were converted into radiant stimulus power. Across both subjects and stimulus sizes we found no differences between threshold power values for both single and cascaded AOM switching (Fig. 5(C)). With a 3x3 pixel stimulus we found a mean threshold power (± standard deviation) of 34.2 ± 5.0 fW (single) and 35.3 ± 7.7 fW (cascade) for S1 ($p = 0.77$), and 17.7 ± 2.1 fW (single) and 19.8 ± 3.6 fW (cascade) for S2 ($p = 0.29$). With the 10x10 pixel stimulus we found a mean threshold power of 35.1 ± 7.3 fW (single) and 39.8 ± 9.2 fW (cascade) for S1 ($p = 0.47$), and 108.7 ± 15.2 fW (single) and 117.2 ± 4.7 fW (cascade) for S2 ($p = 0.43$).
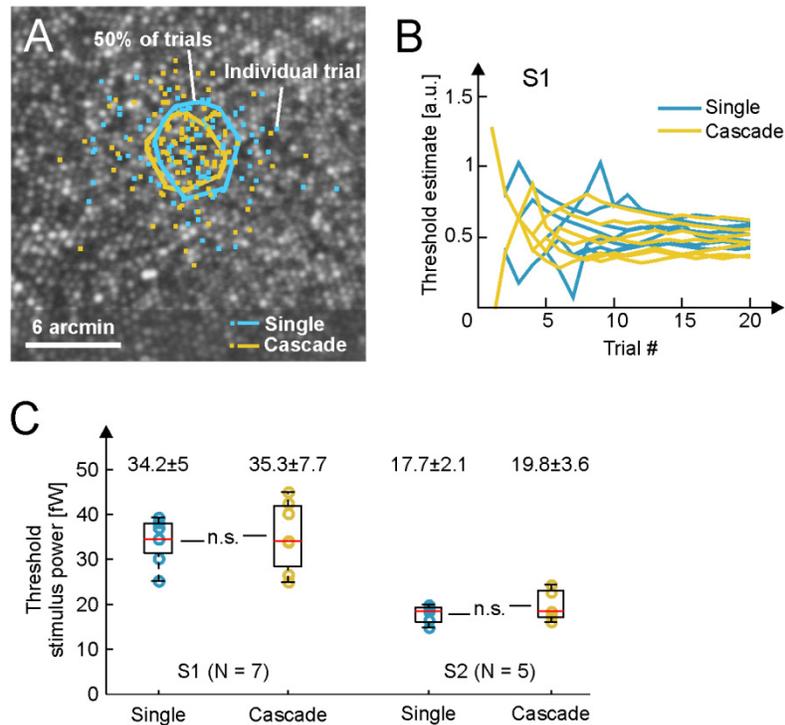
Fig. 5. Psychophysical detection thresholds using single and cascaded AOMs. A: Foveal stimulus locations plotted on S1's AOSLO retinal image in repeated increment sensitivity measurements. Square markers show the exact position and approximate size of the stimulus (3x3 image pixel) for a total of 280 trials. Polygons encompass the area where 50% of all trials hit. Subjects had little fixational eye motion, reflected here by the size of the 50% area. B: Raw psychophysical threshold estimates from the example in A given in arbitrary units of power modulation after 20 trials using QUEST staircases for both single and cascaded AOM switching. Thresholds and variability are similar in both cases. C: Threshold comparison for both single and cascaded switching converted to absolute stimulus power at the cornea in two subjects (S1,S2). We found no significant differences between conditions within subjects (p = 0.77 and 0.29, t-test for paired data). Values indicate mean threshold power in fW ± standard deviation. For all panels, colors denote single (blue) and cascaded (amber) AOM switching, respectively.

4. Discussion

By cascading and temporally aligning two acousto-optic modulators we demonstrate a substantial boost in optical contrast in an SLO-based retinal display, reaching a maximum contrast ratio of about $1:10^{10}$. Using the AOSLO as a retinal display, this superior contrast made it possible to create extremely small stimuli approaching the size of single foveal cones and rods without a visible background, while maintaining a large modulation range for psychophysical testing. We validated our method by recording comparable sensitivity thresholds for stimuli created by the cascade and by a single AOM. High visual contrast has implications for SLO-based displays in particular as well as light switching for high-contrast vision testing in general. Cascaded AOM light switching will extend single cone photoreceptor testing options, and enable single rod testing. These are fundamental applications for both basic and clinical research of retinal function.

Earlier studies reporting maximum contrast ratios in AOM-based displays of around 1:300 are likely to have underestimated the full range of single AOM extinction due to technical difficulties in accurately measuring the AOM's black level (P_{min} in Eq. (1)). Errors can be caused by the use of an unsuited photodiode, or because insufficient cancellation of spurious

light sources in the test setup [6,18,19]. In the current study, we took extra care to avoid both factors: a highly sensitive probe head was employed (see Methods), and outside light sources were eliminated by repeated visual inspection by a human observer after a longer period of dark adaptation. Due to the extremely high extinction ratio of the AOM cascade, we approached the physical limits of silicon photodiode sensitivity to radiant power levels ($\sim 10^{-7}$ mW) in our measurements. Thus, output levels at low drive voltages could only be reported indirectly. Because the attenuation of the cascade can be mathematically described by multiplying the attenuation of its single AOM elements over the full range of measurable output powers (see Fig. 2(A)), we are confident that the maximum contrast values of the cascade reported here are accurate. Further support for this view is provided by the psychophysical results, confirming no difference between single or cascaded AOM operation when both modes are set up to produce comparable light levels (see Fig. 5).

As a byproduct of combining two AOMs with independent drive signals into a single stimulation channel, the amount of displayable light levels (corresponding to the bit depth of the SLO display) increased as well. The system's current hard- and software design allowed single AOM drive signals to be represented in exactly 1,001 steps (~10 bit) between maximal and minimal output. In the cascade, a total of 307,920 unique steps (~18 bit) are theoretically possible to display. Put differently, the cascade expands the range of displayable light levels below the current minimum of 1 ‰ of the maximum intensity and additional light levels between 1 ‰ and 100% can now be set. As a practical note, to display modulated stimuli with cascaded AOMs during threshold experiments, computation of necessary drive signals is simply based on the multiplicative behavior of the cascade (compare Fig. 2). A look-up-table mapping single AOM drive signals to the desired cascade output can be easily established after each single AOM drive to output power relationship has been linearized: if $P_{cascade} = P_{AOM1} \cdot P_{AOM2}$, and $P_{AOM1} = P_{AOM2}$, then $P_{AOM} = \sqrt{P_{cascade}}$. For example, if the desired stimulus intensity is 30% of the maximum intensity, each AOM driving signal is set to a voltage generating an output level of 55% ($\sqrt{0.3} = 0.55$) of the maximum intensity.

Luminance contrast is a key technological characteristic of visual displays which is continuously improving; not only in consumer products but in scientific applications as well. To probe visual function of the intact human visual system, the physical requirements for stimulation devices and displays are high and frequently unmet by off-the-shelf solutions. In most of today's psychophysical studies of human vision, cathode ray tubes (CRTs) are still the display of choice, because of their high temporal and spatial fidelity and custom control of their source electron guns [20]. CRTs can produce visual contrast ratios of up to $1:10^4$, on par with liquid crystal displays (LCD) [21]. Higher contrasts of up to $1:10^{6.7}$ can be found in organic light emission diode (OLED) displays [22]. Similar high-contrast ratios of about $1:10^{6.4}$ can be achieved in projector systems with two conjugate digital mirror device (DMD) units [23]. For SLO-based displays, a few alternatives to AOM light intensity modulation exist. Bright light sources such as super luminescent laser diodes (SLDs, e.g. model iBeam-smart, TOPTICA Photonics AG, Munich, Germany) can be electronically modulated fast enough [24], but are bound to their diode's wavelength and options are (yet) too limited for psychophysical testing. For example, there is currently no laser diode with a central wavelength close to 550 nm, which would minimize sensitivity differences in M- and L-cone photoreceptors [25]. Other fast optical switches can be established by electro-optical modulation (e.g. model EO-AM-NR-C4, Thorlabs GmbH, Dachau, Germany) or pockels cells (e.g. model EO-PC-550, Thorlabs), but both options have lower contrast ratios when compared to AOMs (EO-AM: $1:10^1$, EO-PC: $1:10^{2.4}$) [26].

As exemplified in the current study, an SLO-based display with AOM cascading can produce spatially resolved stimuli with visual contrast ratios up to $1:10^{10}$. To the best of our knowledge, this is the highest visual contrast ever reported in any display device. With the added minute spatial and temporal control of a small visual stimulus, this system is well

suited to stimulate individual cone and rod photoreceptors against a zero-luminance background. For instance, if source light levels are decreased appropriately (e.g. by neutral density filters), the AOM cascade described here can produce background light levels well below the detection threshold of cone and rod photoreceptors. The detection threshold for cones is about 200 incident photons with a wavelength $\lambda = 490$ nm at an integration time $t = 100$ ms [27]. This is equivalent to 225 photons at 543 nm. With the Planck constant, h ($6.26 \cdot 10^{-34}$ Js), the speed of light, c ($3 \cdot 10^{-8}$ m / s), number of photons, n_γ, wavelength, λ, and integration time, t, this equates, according to Eq. (4), to a radiant threshold power of $P_{cone} = 8.23 \cdot 10^{-16}$ W,

$$P_{cone} = \frac{h \cdot c \cdot n_\gamma}{t \cdot \lambda}, \tag{4}$$

which compares well to our foveal detection threshold estimate of the background light of about $1.8 \cdot 10^{-15}$ W. For rods, detection of single photons have been reported, and thresholds are likely to be somewhere around 50 incident photons [27,28], thus around $6.76 \cdot 10^{-17}$ W. This is close to our estimated threshold at 10° eccentricity (where the density of rod photoreceptors is highest) of $6.3 \cdot 10^{-17}$ W in cascaded viewing condition. If the minimum output power of the cascade is attenuated with a 1 log unit ND filter to produce a background of $P_{min} = 8.4 \cdot 10^{-17}$ W – an order of magnitude below the detection threshold of single cones – the maximum output power in this scenario would be $P_{max} = 1 \mu W$. The smallest square stimulus in the current AOSLO system (2 x 2 pixel) at 543 nm would result in a luminance of $L_v = 3.1 \cdot 10^{-2}$ cd/m^2, (~1 Troland at a 7 mm pupil) which is clearly visible. For rod photoreceptors, light levels can be adjusted accordingly.

A zero-background stimulation channel is an important step towards new experimental options, but for some applications, the concurrent imaging raster has to be invisible as well. In our case, using 840 nm as imaging wavelength (at power levels suited for imaging, ~0.1 mW at the cornea), the imaging field produces an equivalent scotopic luminance of ~3.14 cd/m^2. One solution would be to shift imaging towards longer, less visible wavelengths (in conjunction with appropriate detectors), or suspend imaging for experimentation times, and recover stimulus locations from external, invisible methods, such as high-resolution IR pupil trackers [29]. A considerable drawback of the cascade is the overall light loss of 90% compared to single AOM operation. This reduction of maximum radiant power output needs to be taken into account in applications where light levels are a limiting factor.

Single photoreceptor psychophysical testing has recently proven to offer new insights into retinal function on the elemental level of single cells. In previous experiments, this was realized by single AOM switching, creating small visual stimuli within a visible background. This background light set fundamental limits to experimental designs. For example, single cone sensitivity thresholds are necessarily reported as thresholds to light increments [6,15,17]. In a study of single cone color appearance, background light options were limited, requiring high intensity fields to mask the residual background of the stimulus light [16]. By cascading two AOMs we can now extend experimental options enabling background-free, high-contrast ($1:10^{10}$) visual stimulation. In color vision applications, this approach will allow photoreceptor function tests with a greater freedom for custom adaptation lights, and a zero background situation will enable isolated stimulation of single cones for extended cone-resolved models of color computation [30]. In clinical applications, the higher dynamic range of stimulus lights will enable dark adapted vision- as well as rod function testing. Rod function testing is of importance for clinically oriented visual testing [15,31,32], especially with regard to retinal diseases affecting mesopic and scotopic vision, where early signs of the disease is most likely found in reduced rod function [33,34].

Appendix

Conversion from radiant power to equivalent luminance in the AOSLO

Based on radiant power measurements of the AOSLO beam at the subject's pupil position, we calculated the equivalent luminance (in cd/m^2 or Troland) of the background field of the AOSLO, similar to [35], as follows:

1) Due to measurement limitations at very low light levels, radiant power at the pupil was measured with a maximum drive signal (1 V) with 100% duty cycle (for light safety, the duty cycle is kept at 40% during imaging and stimulation).

2) Background light (leak) radiant power P_{min} was determined by applying the AOM specific voltage-power characteristic for $U = 0$ found earlier (see Eq. (2)).

3) Luminous flux Φ [lm] is calculated by:

$$\Phi = K_m \left[\frac{lm}{W} \right] \cdot P_{min} [W] \cdot V(\lambda)$$

3) With $K'_m = 1700 \; \dfrac{lm}{W}$ (scotopic vision) and $K_m = 683 \; \dfrac{lm}{W}$ (photopic vision). P_{min} is the AOM output power and $V(\lambda)$ describes the luminous efficiency of human vision (use $V'(\lambda)$ for scotopic vision).

4) The retinal illuminance $E_R \left[\dfrac{lm}{m^2} \right]$ is calculated based on the retinal area A_R [m^2] subtended by the scan field:

$$E_R = \frac{\Phi[lm]}{A_R[m^2]}$$

The retinal area A_R [m^2] depends on the scan angle θ of the AOSLO system and we assume the standard emmetropic distance f_e [m] of the human eye:

$$A_R = \left(2 \cdot \tan\left(\frac{\theta}{2} \right) \cdot f_e[m] \right)^2$$

5) For converting illuminance, E_R, into luminance, $L_v \left[\dfrac{cd}{m^2} \right]$, we assume that the source (the pupil) is uniform such that the light in the solid angle to the source is equal to the light in the same angle from the source. Hence

$$L_v = E_R \left[\frac{lm}{m^2} \right] \cdot \frac{\left(f_e[m] \right)^2}{A_P \left[m^2 \right]},$$

with pupil area $A_P[m^2]$.

6) The Troland T [td] is simply calculated by:

$$T = L_v \left[\frac{cd}{m^2} \right] \cdot A_P \left[mm^2 \right]$$

Examples

The following values are used in both examples:

Emmetropic distance, $f_e = 1.67 \cdot 10^{-2}\, m$

Scan angle, $\theta = 0.85°$

Pupil area, $A_P = 38.5\, mm^2$

a) Background detection threshold: The background light intensity of the stimulation channel is around $P_{min} = 1 \cdot 10^{-16}\, W$ and the scotopic luminous efficiency is $V'(\lambda = 543\, nm) = 0.599$. Using this parameters one will find:

$$L_v = \frac{K'_m \left[\frac{lm}{W}\right] \cdot P_{min}[W] \cdot V'(\lambda = 543\, nm)}{\left(2 \cdot \tan(\frac{\theta}{2}) \cdot f_e[m]\right)^2} \cdot \frac{(f_e[m])^2}{A_P[m^2]} = 4,82 \cdot 10^{-6}\, \frac{cd}{m^2}$$

b) Imaging raster

The 840 nm imaging raster with a power of $P = 100\ \mu W$ at the cornea is clearly visible and resides in the realm of photopic vision. We extrapolated the luminous efficiency at that wavelength by a logarithmic fit to the data from Stockman and Sharpe [36] to find $V(\lambda = 840\, nm) = 3.89 \cdot 10^{-7}$. Therefore the equivalent luminance of the imaging field is:

$$L_v = \frac{K_m \left[\frac{lm}{W}\right] \cdot P[W] \cdot V(\lambda = 840\, nm)}{\left(2 \cdot \tan(\frac{\theta}{2}) \cdot f_e[m]\right)^2} \cdot \frac{(f_e[m])^2}{A_P[m^2]} = 3.14\, \frac{cd}{m^2}$$

Disclosures

AR: USPTO#7,118,216, "Method and apparatus for using AO in a scanning laser ophthalmoscope" and USPTO #6,890,076, "Method and apparatus for using AO in a scanning laser ophthalmoscope". These patents are assigned to both the University of Rochester and the University of Houston and are currently licensed to Canon, Inc. Japan. Both AR and the company may benefit financially from the publication of this research.